Stabilization and Thickness Dependence of Depletion Charge Induced Domains in Ferroelectric Nano Capacitors

I. B. Misirlioglu, M. Yildiz
Faculty of Engineering and Natural Sciences, Sabancı University
Istanbul, Turkey

***Abstract*—We analyze the domain structures as well as the phase transition temperatures in films with depletion charges. Due to depletion charges, saw-tooth like domain structures can develop spanning the entire film thickness in films with perfect electrode screening, i. e., ideal electrodes if the film is above a critical thickness. Transition temperature in films with dead layers does not depend nearly at all on the depletion charge density unless it is very high (>10^{26} ionized impurities/m^3). Relatively thick films (>8 nm in this work) with dead layers that have very high depletion charge densities have transition temperatures similar to those with the same charge density but with ideal electrodes, making us conclude that thick films with high depletion charge densities will not feel the dead layer effects. The results are provided for (001) $BaTiO_3$ films grown on (001) $SrTiO_3$ substrates with pseudomorphic top and bottom metallic electrodes.**

Keywords- Ferroelectric films, depletion charge, electrostatics, phase transition, thermodynamic simulation

I. INTRODUCTION

The intrinsic limit of ferroelectricity in thin films has been a topic of extensive discussions in many reports. Formation of a charged region and the consequent effects in ferroelectric films has been mostly analyzed experimentally in addition to a few theroetical studies [1-5, 11] including attempts in artifically graded structures [6]. Understanding the evolution of these charges under limited lattice diffusivities but how such phenomena will be impacted by interface effects has also been emphasized [5]. In a real ultrathin ferroelectric film, its thickness, when at the order of a few tens of nm or less, can be comparable or smaller than the depletion zone width in a ferroelectric in contact with electrodes that has typical densities of impurities. Thus ,the entire ultrathin film can be said to be depleted. Depletion widths of around 30 nm and ionized impurity densities of around $10^{25\text{-}27}/m^3$ have been reported by Pintilie *et al*. using interfacial capacitance measurements for $PbZr_{0.2}Ti_{0.8}O_3$ films [4].

Existing studies analyze the effects of continuous depletion charge distributions on the observable properties in relatively thick films [1, 3, 6-7] in the single domain state. The possibility that, due to the inhomogeneous nature of the system owing to depletion charges, the transition could be into multidomain states even in structures with ideal electrodes would make a prominent difference in the calculated transition temperatures, which is one of the main emphasis given in this work. One could easily foresee that the conclusions withdrawn for systems with ideal electrodes will have to be modified, for instance, for systems that have imperfect film-electrode interfaces, namely real electrodes.

To address the depletion charge effects, we use the Landau-Ginzburg-Devonshire (LGD) formalism for a ferroelectric film coupled with the interface conditions and presence of depletion charges. At high depletion charge densities, domains with a saw-tooth type structure form regardless of the presence of the dead layers at the film-electrode interfaces and that dead layer effects, if present, dominate at low thicknesses. Our results reveal the magnitudes of changes that can be expected in the transition temperatures for films with depletion charges considering particularly the transition into multidomain states.

II. THEORY AND METHOD

The schematic of the geometry considered is given in Figure 1. A two dimensional grid is constructed that has 200*n* x *kn* cells where *k* (200) is the number of cells along the film thickness (width) and each cell, *n*, has a dimension of 0.4 nm, nearly the lattice parameters of well known pseudocubic perovskites such as BT to imitate the order of lengths at which *P* can vary in the system compared to real systems. The equations of state are derived from the LGD free energy for all *P* in our system for an epitaxial monodomain (001) $BaTiO_3$ ferroelectric film on a (001) $SrTiO_3$ cubic substrate along with

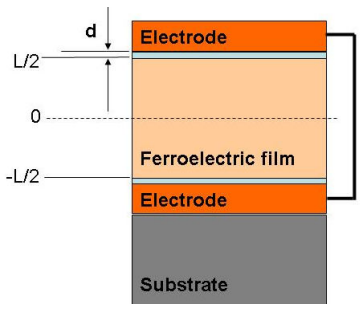

Figure 1. (Color Online) The schematic of the ferroelectric thin film capacitor considered in this study.

the Maxwell equation for dielectric displacement employing a finite difference discretization. We partition the thin film capacitor system along the thickness axis, *z*, as follows:

$$w=1 \text{ when } -h/2 \le z \le +h/2$$
$$w=0 \text{ when } -h/2-d < z < -h/2 \text{ and } +h/2 < z < d+h/2, \quad (1)$$

where *w* is a step-wise function defining the interface between the dead layer and the ferroelectric and *d* is the dead layer thickness (1 unit cell, ~0.4 nm in this work), |*h*| is the thickness of the ferroelectric layer. The electrode-dead layer interfaces are at $-h/2-d$ and $d+h/2$ respectively. Note that $\boldsymbol{d}=0$ indicates a perfect film-electrode contact interface. The equations of state for the system using the definition of *w* in (1) are,

$$\begin{aligned} &w(2\alpha_3^m P_3 + 4\alpha_{13}^m P_3 P_1^2 + 4\alpha_{33}^m P_3^3 + 6\alpha_{111} P_3^5 \\ &+ \alpha_{112}(4P_3 P_1^4 + 8P_3^3 P_1^2) + 2\alpha_{123} P_3 P_1^4 - G_{33}\frac{d^2 P_3}{dz^2} - G_{13}\frac{d^2 P_3}{dx^2}) + (1-w)\frac{D_3}{\varepsilon_r \varepsilon_0} \\ &= wE_3^F + (1-w)E_3^d \end{aligned} \quad (2a)$$

$$\begin{aligned} &w(2\alpha_1^m P_1 + 2(2\alpha_{11}^m + \alpha_{12}^m)P_1^3 + 2\alpha_{13}^m P_1 P_3^2 + 6\alpha_{111} P_1^5 + \\ &2\alpha_{112}[3P_1^5 + 3P_1^3 P_3^2 + P_1 P_3^4] + 2\alpha_{123} P_1^3 P_3^2 - G_{31}\frac{d^2 P_1}{dz^2} + G_{11}\frac{d^2 P_1}{dx^2}) + (1-w)\frac{D_1}{\varepsilon_r \varepsilon_0} \\ &= wE_1^F + (1-w)E_1^d \end{aligned} \quad (2b)$$

where P_i (i=1,2,3) are the components of *P* in the ferroelectric state, α_3^m, α_{13}^m, α_{33}^m, $\boldsymbol{\alpha_1^m}$, $\boldsymbol{\alpha_{11}^m}$, $\boldsymbol{\alpha_{12}^m}$ are the renormalized dielectric stiffness coefficients, modified by the misfit strain and the two-dimensional clamping of the film, while $\boldsymbol{\alpha}_{111}$, $\boldsymbol{\alpha}_{112}$, $\boldsymbol{\alpha}_{123}$ are the dielectric stiffness coefficients in the bulk [8], G_{ij} are the gradient energy coefficients and are assumed isotropic, $G_{ij}=G=3\text{x}10^{-10}$. We also neglect the gradients in P_2 along *y* within the two dimensional limit. $\boldsymbol{E_3^F}$, $\boldsymbol{E_1^F}$ and $\boldsymbol{E_3^d}$, $\boldsymbol{E_1^d}$ are the fields along *z*- and *x*-axis in the ferroelectric layer and the dead layer respectively. The equality between the field and the dielectric displacement in the dead layer (w=0) reads $\boldsymbol{D_3 = \varepsilon_r \varepsilon_0 E_3^d}$ and $\boldsymbol{D_1 = \varepsilon_r \varepsilon_0 E_1^d}$ and for w=1 (ferroelectric layer), $\boldsymbol{D_3 = \varepsilon_b \varepsilon_0 E_3^F + P_3}$ and $\boldsymbol{D_1 = \varepsilon_b \varepsilon_0 E_1^F + P_1}$. The dead layer, when present, is a high-*k* dielectric whose dielectric constant, ε_r, is 20 to exemplify its effects and ε_b is the background dielectric constant of the ferroelectric (taken as 7 in this work). The electric fields in both the ferroelectric layer and the dead layer are

$$\boldsymbol{E_3^F = -\frac{d\phi^F}{dz}},\ \boldsymbol{E_1^F = -\frac{d\phi^F}{dx}}, \quad (3)$$

for the ferroelectric and

$$\boldsymbol{E_3^d = -\frac{d\phi^d}{dz}},\ \boldsymbol{E_1^d = -\frac{d\phi^d}{dx}}. \quad (4)$$

in the dead layers with $\boldsymbol{\phi^F}$ and $\boldsymbol{\phi^d}$ being the electrostatic potential in the ferroelectric and the dead layer respectively. Using the Maxwell relation $\nabla \cdot D = \rho$ when depletion charges due to ionized impurities are present, one has

$$\boldsymbol{\frac{d^2\phi^F}{dz^2} + \frac{d^2\phi^F}{dx^2} = \frac{1}{\varepsilon_b \varepsilon_0}\left(\frac{dP_3}{dz} + \frac{dP_1}{dx} - \rho\right)},\ \boldsymbol{\frac{d^2\phi^d}{dz^2} + \frac{d^2\phi^d}{dx^2} = \frac{\rho}{\varepsilon_r \varepsilon_0}} \quad (5)$$

in the ferroelectric layer and dead layer respectively.We assume that each impurity contributing to $\boldsymbol{\rho}$ has only one positive unit charge (the charge of one electron). The depletion charge density in this work is assumed to be constant throughout the film volume [3, 4] the boundary conditions we employed for $P_{1,3}$ are

$$\left[P_1 + \lambda\frac{dP_1}{dz}\right]_{z=-\frac{h}{2}-d,\frac{h}{2}+d} = 0,\ \left[P_3 + \lambda\frac{dP_3}{dz}\right]_{z=-\frac{h}{2}-d,\frac{h}{2}+d} = 0 \quad (6)$$

at the top and bottom interfaces of the ferroelectric where the extrapolation length, λ, is taken as infinite. Periodic boundary conditions are used along the *x*-axis, i. e., $P_3(z, x=0) = P_3(z, x=L)$ $P_1(z, x=0) = P_1(z, x=L)$ .We apply Dirichlet boundary conditions to solve *P* in the thin film capacitors. At the dead layer-electrode interfaces, $\boldsymbol{\phi}$ =0 correspond to total charge compensation at the film-electrode interface while periodic boundaries are adopted along *x*. Equations of state (2a-2b) along with the equations of electrostatics in (7) are solved simultaneously for *P* components employing a Gauss-Seidel iterative scheme. We limit ourselves to 10000 iterations converging to a difference of about 10^{-8} between consecutive iterative steps. Compressive in-plane misfit in (001) $BaTiO_3$ on (001) $SrTiO_3$ is about 2.5 % and only P_3 is the spontaneous polarization that, when depletion charge exists, also contain the built-in polarization, P_b or else $P_3 = P_f$. From here onwards the ferroelectric part of P_3 will be denoted as P_f and the built-in part as P_b.

III. RESULTS AND DISCUSSION

A. Room temperature domain structures when d=0

Room temperature (RT) structures with that are thinner than 10 nm thickness are nearly always found to exist in an imprinted single domain state and is not of interest here. The films without any depletion charge also exist in a homogeneous monodomain state and are not discussed. Depletion charge densities as high as $10^{25\text{-}27}$ ionized impurities/m^3 were reported [4] and we remain around these ($2\text{x}10^{26}$ for the high limit) values in our simulations. In Figure 2, we give the total polarization in the 12, 16 and 20 nm films that have a fixed volumetric depletion charge density corresponding to $2\text{x}10^{26}$ ionized impurties/m^3

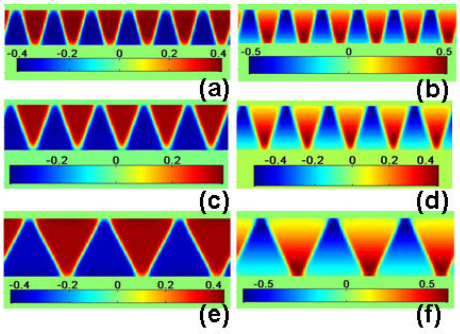

Figure 2. (Color Online) The RT domain total polarization configurations of the (a) 12 nm, (b)16 nm and (c) 20 nm thick films with $2x10^{26}$ ionized impurities/m^3 and the extracted ferroelectric polarization given for (d) 12, (e)16 and (f) 20 nm thick films on the right hand side. Scales are given to display the range of P_3 in C/m^2.

along with the ferroelectric polarization and the latter is obtained by subtracting P_b from P_3 for 12 nm, 16 nm and 20 nm films. The P_b is found by calculations above the Curie point as it is nearly temperature insensitive and is the only solution satisfying (2a-2b). At $2x10^{26}$ ionized impurities/m^3, a saw-tooth type domain pattern develops at RT whose period is a function of thickness. Relatively lower depletion charge densities (<10^{26} ionized impurities/m^3) do not tend to stabilize domains and result in a uniaxial P_f. Therefore, domains in thicker films are due to the highly inhomogeneous built-in field renormalizing the linear term in P_3 in (2a). Thicker structures are forced to undergo domain stabilization to minimize the depolarizing fields emanating from the greater extent of the inhomogeneous depletion charge field as schematically depicted in Figure 3 for clarity.

B. Room temperature domain structures when d=1

In the presence of dead layers (d=1 unit cell) and depletion charge, a competition between the two formations, each of which is a source of inhomogeneity, takes place. A set of structures at RT for three different thicknesses and two depletion charge densities are provided in Figure 4. The left hand side gives the domain structure in the absence of depletion charge while the right hand side is when depletion charge is present. Subtracting the P_b at each site from P_3, we get the P_f as we did in the previous section. Relatively high density of depletion charge ($2x10^{26}$ ionized impurities/m^3) alters the domain wall angles with respect to the film normal along with a period change. It is instructive to discuss behavior to plot and compare the wave vector k of domains ($k=2\pi/\lambda$ where λ is domain period) as a function of thickness as we do in Figure 4. Here, we first give the results for the domain wave vector, k, we obtained both in our simulations and using the approach in Refs. 10-11 to validate the trends of our simulations for charge-free films in Figure 5a. We find that the domain period does not nearly change at all with further cooling upon the transition from the paraelectric to the multidomain FE state. The system transforms from a sinusoidal pattern to a square-like one, making it feasible to compare k values at and below the transition.

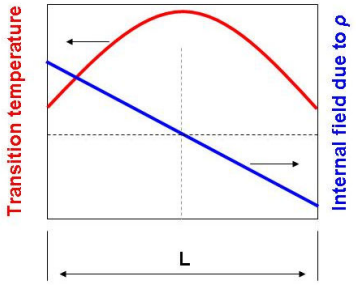

Figure 3. (Color Online) Schematic of the built-in field and local transition temperature plotted as a function of position along the thickness of the ferroelectric film for a given homogeneous charge density.

It is instructive to discuss behavior of the wave vector, k of the P_f wave plotted as a function of film thickness for ionized impurity densities of $5x10^{25}$ and $2x10^{26}$ /m^3 in Figure 5b. The presence of electrical domains in films with depletion charge have persisted for the entire thickness range of interest in our study. Domain period for films thinner than 12 nm with $5x10^{25}$ ionized impurities/m^3 is smaller than the charge-free film, while $2x10^{26}$ ionized impurities/m^3 follows more or less the charge-free film but with slightly larger k values. But this trend changes with increasing film thickness for the films having $5x10^{25}$ ionized impurities/m^3 with respect to the charge-free case. From the result of our simulations, we can see that the domain period is altered in a way leading to a finer domain period hence a larger k.

C. Phase transition temperatures

The paraelectric-ferroelectric transition temperatures for films with depletion charge is expected to be lowered in the presence of depletion charges, dead layers or when both coexist. For reference, we first computed the transition temperature as a function of film thickness for a fixed dead layer thickness (d=1) and dielectric constant (ε_r=20) and our results are in Figure 6a along with the results we obtained using the method prescribed in Refs. 10-11. We find the transition temperatures by tracking <|P_3|>. It must be borne in mind that the approach of Refs. 10-11 excludes the gradient of

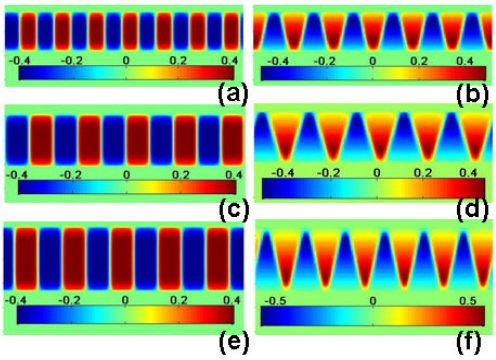

Figure 4. (Color Online) Domain structures for (a) 12 nm, (b) 16 nm and (c) 20 nm thick films with dead layers. The right hand side of each colormap for a given thickness are the domain structures for ρ=$2x10^{26}$. Scales are given to display the range of P_3 in C/m^2.

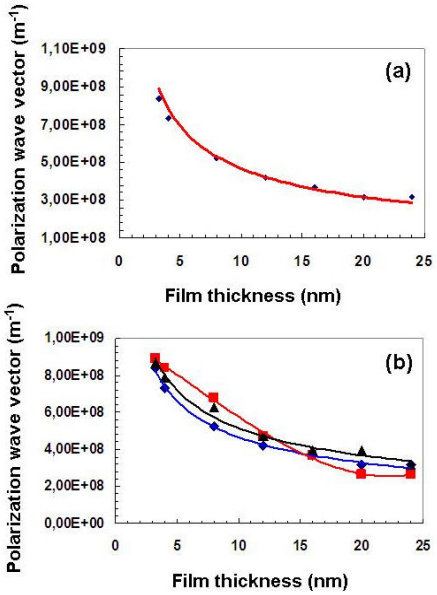

Figure 5. (Color Online) (a) Wave vector of the polarization along the film plane as a function of film thickness at the transition found using the method of Refs. 10-11 and the wave vector we found in our simulations (blue squares) for d=1 unit cell. (b) Wave vector of the polarization along the film plane as a function of thickness for films without charge (blue curve with diamonds), films having $5x10^{25}$ ionized impurities/m^3 charge density (red curve with squares) and films having $2x10^{26}$ ionized impurities/m^3 charge density (black curve with triangles) for d=1 unit cell. The curves in (b) are guides for the eyes.

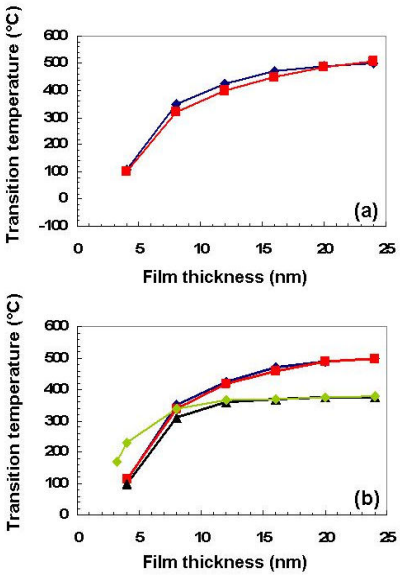

Figure 6. (Color Online) (a) Transition temperatures in films with dead layers as a function of thickness when no charge is present. The blue curve with diamonds indicate simulations and the red curve with squares are the results obtained using the method in Refs. 10-11. (b) Comparison of the results for charge-free (blue curve with diamonds), films having $5x10^{25}$ ionized impurities/m^3 (red curve with squares), films having $2x10^{26}$ ionized impurities/m^3 depletion charge (black curve with triangles) and the green curve with triangles is the case for d=0 (no dead layer) and $2x10^{26}$ ionized impurities/m^3 depletion charge given for comparison. The bulk transition temperature for (001)$BaTiO_3$ fully strained on (001)$SrTiO_3$ is 615°C.

P_3 along the thickness of the film, which we do include in our study. This can be the possible cause of the slight deviation between the two results at small thicknesses. Decreasing film thickness results in a reduction of the transition temperature with domain period subsequently becoming comparable or larger than the film thickness. We do not go down to very low temperatures corresponding to below 3.2 nm in this work. In films with dead layers, we note that films with a charge density of $5x10^{25}$ ionized impurities/m^3 have nearly the same transition temperature compared to the charge free ones for a given thickness (See Figure 6b). A homogeneous charge distribution does not lead to any net bias fields between the electrodes and no smearing of the transition exists. The films with $2x10^{26}$ ionized impurities/m^3 and dead layers have a similar trend with the charge-free films at small thickness but the transition temperature is significantly reduced for thicker films. Moreover, the transition temperatures in thicker films with and without dead layers are nearly the same. This scenario is certainly different for thinner films (<12 nm) and it is seen that the dead layers entirely dominate the transition characteristics (Compare the curves for the films having $2x10^{26}$ ionized impurities/m^3 with and without dead layers in Figure 6b). Therefore, we provide quantitative evidence that thicker films will be under a much stronger influence of depletion charges compared to thinner ones. The former will nearly not feel dead layer effects and domains might arise even in the presence of ideal electrodes.

REFERENCES

[1] A. N. Morozovska and E. A. Eliseev, "Modelling of dielectric hysteresis loops in ferroelectric semiconductors with charged defects", J. Phys: Cond. Mat., vol. 16, pp. 8937-8956, 2004.

[2] A. M. Bratkovsky and A. P. Levanyuk, "Ferroelectric phase transitions in films with depletion charge", Phys. Rev. B., vol. 61, pp. 15042-15050, 2000.

[3] H. Matsuura, "Calculation of band bending in ferroelectric semiconductor" New. J. Phys., vol. 2, pp.81-811, 2000.

[4] L. Pintilie and M. Alexe, "Metal-ferroelectric-metal heterostructures with Schottky contacts. I. Influence of the ferroelectric properties" J. Appl. Phys., vol. 98, pp. 124103-8, 2005.

[5] Xiao Y., Shenoy V. B. and Bhattacharya K., "Depletion layers and domain walls in semiconducting ferroelectric thin films", Phys. Rev. Lett., vol. 95, pp. 247603-4, 2005.

[6] M. B. Okatan, J. V. Mantese and S. P. Alpay, "Effect of space charge on the polarization hysteresis characteristics of monolithic and compositionally graded ferroelectrics", Acta Mat., vol. 58, pp. 39-48, 2010.

[7] I. B. Misirlioglu, M. B. Okatan and S. P. Alpay, "Asymmetric hysteresis loops and smearing of the dielectric anomaly at the transition temperature due to space charges in ferroelectric thin films", J. Appl. Phys., vol. 108, pp.034105-8, 2010.

[8] These coefficients are compiled from "N. A. Pertsev., A. G. Zembilgotov and A. K. Tagantsev, "Effect of mechanical boundary conditions on phase diagrams of epitaxial ferroelectric thin films", Phys. Rev. Lett., vol. 80, pp. 1988-1991, 1998."

[9] M. B. Okatan, A. L. Roytburd, J. V. Mantese and S. P. Alpay., "Domain engineering in compositionally graded ferroelectric films for enhanced dielectric response and tunability", J. Appl. Phys., vol. 105, pp.114106-9, 2009.

[10] E. V. Chensky and V. V. Tarasenko, "Theory of phase transitions into inhomogeneous states in finite ferroelectrics in an external field", Zh. Eksp. Teor. Fiz., vol. 83, pp.1089-1099, 1982.

[11] A. S. Sidorkin, *Domain Structure in Ferroelectrics and Related Materials*, Cambridge Int. Science Publishing, (2006).